KINETIC ANALYSIS OF SODIUM CHANNEL BLOCK BY INTERNAL METHYLENE BLUE IN PRONASED CRAYFISH GIANT AXONS

JOHN G. STARKUS, STEVEN T. HEGGENESS, AND MARTIN D. RAYNER
Békésy Laboratory of Neurobiology, Pacific Biomedical Research Center and the Department of Physiology, John A. Burns School of Medicine, University of Hawaii, Honolulu, Hawaii 96822

ABSTRACT The cationic dye methylene blue (MB^+) blocks I_{Na} in a voltage and time-dependent manner and exhibits no frequency dependent block at 1 Hz when internally perfused in normal or pronase-treated crayfish axons. Peak I_{Na} decreases with increasing MB^+ concentrations in the range 50 μM to 5 mM, but the blocking time constant approaches an asymptote at concentrations above 500 μM. I_gON is not noticeably affected by internal MB^+ at concentrations of 500 μM or below, in the absence of external tetrodotoxin (TTX). However, 5 mM MB^+ produces a visible suppression of I_gON that is reversible following washout. A pseudo–first-order analysis of MB^+ blocking kinetics suggests a drug binding site deep in the transmembrane voltage field (dz = 0.85, K_D = 11 μM at 0 mV). The voltage sensitivity of the individual rate constants is highly asymmetric, suggesting that the major energy barrier for MB^+ is very close to the axoplasmic margin of the voltage field. Reversing the Na^+ gradient and direction of I_{Na} has little effect on the kinetics of MB^+ block. The kinetic properties of state-dependent vs. state-independent blocking schemes are investigated and compared with our observations of MB^+ block. Analysis of hooked sodium tail currents following depolarization to various test potentials demonstrates quantitatively that MB^+ binds in a state-dependent manner to open sodium channels. The appropriateness of first-order kinetic analysis of drug block is then considered in light of these observations.

INTRODUCTION

Following the approach introduced by Woodhull (1973) for analysis of voltage-dependent sodium pore block by permeant H^+ and Ca^{++} ions, Strichartz (1973) investigated voltage-sensitive local anesthetic block by internally applied lidocaine derivatives. He concluded that such blocks only occur in pores with open m and h gates and uses a pseudo–first-order model to show that voltage-dependent binding of QX314 and QX222 occurs deep within the voltage gradient across the open sodium pores. This model has since been widely adopted for description of voltage-sensitive block in sodium channels by "open pore" blocking agents (e.g., Courtney, 1975; Hille, 1977; Yeh and Narahashi, 1977; Cahalan, 1978; Yeh, 1979; and Cahalan and Almers, 1979*a*,*b*).

Several observations have suggested additional complexity in the blocking reaction. Yeh and Narahashi (1977) noted a marked asymmetry between the voltage sensitivity of the forward and back reactions for pancuronium binding. In addition, Yeh (1979) has suggested that 9 aminoacridine (9AA) binds to pronased axons with greater voltage sensitivity at negative potentials than at positive potentials. Furthermore, Lo and Shrager (1981*a*, *b*) have demonstrated saturation of the rate of *N*-propylguanidinium (nPG) binding at high drug concentrations. This last observation is inconsistent with any pseudo–first-order model. The present paper seeks to further clarify the nature of sodium pore block by detailed study of the kinetics of methylene blue (MB^+) binding.

Voltage-sensitive, sodium pore block has been subdivided into a number of different components that may well have different mechanisms of action and different binding sites. Cahalan et al. (1980) distinguish pronase-sensitive "inactivation enhancers" from pronase-insensitive "gate immobilizing" agents. Similarly, Yeh (1979) working with 9AA, has noted both "initial" and "frequency-dependent" components of block in nonpronased axons and "time-dependent" voltage sensitive block in pronased axons.

MB^+ was chosen for this study in view of the relatively simple parameters of block that occur at the dye concentrations principally investigated here. MB^+ block of sodium current is pronase insensitive and time dependent but shows no marked frequency dependence even in nonpronased axons. It seemed possible, therefore, that careful quantitative analysis of the rate and extent of MB^+ block

Dr. John G. Starkus, Pacific Biomedical Research Center, Békésy Laboratory of Neurobiology, University of Hawaii, 1993 East West Road, Honolulu, Hawaii 96822. USENET:(ihnp4!islenet!bigtuna!john).

might provide clear evidence as to the underlying mechanism of the time-dependent component of local anesthetic action.

METHODS

Medial giant axons from the crayfish, *Procambarus clarkii*, were internally perfused and voltage clamped using methods previously described (Shrager, 1974; Starkus and Shrager, 1978). Series resistance compensation for 10 $\Omega \cdot cm^2$ was utilized. Junction potentials of ~8 mV, between measuring potential electrodes, were corrected for at the beginning of each experiment. Temperature was controlled by Peltier devices (Cambion Corp., Cambridge, MA) and was measured with a thermilinear thermistor (Yellow Springs Instrument, Co., Yellow Springs, OH) and set to 6.0 ± 0.1°C. Electrode potential drift, measured at the end of each experiment rarely exceeded 3 to 5 mV even after 4 to 7 h of data recording.

Data Recording and Signal Averaging

Membrane currents were digitized with 12-bit resolution using a Nicolet 1090A digital oscilloscope (Nicolet Instrument Corp., Madison, WI) and then transferred to the Nicolet 1170 for signal averaging. The range of sample rates utilized varied from 0.5 to 5 μs per point for a total of 4,096 points. Unless otherwise noted, all data traces have been signal averaged. The final average was stored on floppy disks utilizing the Ohio Scientific Microcomputer C3-SI (Ohio Scientific Inc., Aurora, OH).

Voltage-clamp pulses were generated by a 12-bit digital-to-analog programmable pulse generator (Adtech Inc., Honolulu, HI), which was under microcomputer control. Direct subtraction of linear capacity and leak currents was achieved for each sodium current record by alternating and summing depolarizing test pulses with hyperpolarizing P/n pulses (Starkus et al., 1981). For pronase-treated axons, hyperpolarizing P/n pulses were pulsed from a base of −130 mV to a maximum of −180 mV. Data analysis was carried out utilizing both the OSI microcomputer (Ohio Scientific Inc.) and the data processing features on the Nicolet 1170 (Nicolet Instrument Corp.). Illustrations were obtained using a digital plotter (HI Plot, Houston Instruments, Austin, TX).

Pronase Treatment

Although removal of sodium inactivation by pronase treatment has been successfully achieved in squid and other axons, we know of no previous report of its successful utilization in crayfish axons. Pronase from *Streptomyces griseus* at a concentration of 0.5 mg/ml was typically added to the cesium perfusate immediately before pronasing. After 10 min this procedure was repeated with a second freshly prepared pronase solution. Pronase treatment removed most of the normal inactivation but some inactivation always remains.

Two major problems can occur in crayfish axons after pronase treatment First, rundown or loss of sodium channels occurs more rapidly in pronased axons. Typically, in normal axons with intact inactivation, only ~10% loss of sodium current occurs after 2 h, whereas 50% rundown is common in pronased axons over a comparable period of time. Therefore, the effects of MB^+ in pronased axons were assessed by comparison with control records taken immediately before and after each application of MB^+. Any small rundown occurring within each period of drug exposure (usually 5 to 10%) was then corrected by scaling for loss in gating-current magnitude. In the absence of external TTX, MB^+ (500 μm and below) does not affect the initial magnitude of gating current (see Fig. 2 *A*, *B* and Armstrong and Croop, 1982). Furthermore comparison of control records taken at different times throughout our experiments makes clear that, following pronase washout, the ratio, I_gON/I_{Na}, is not affected by the rundown process. A second problem often associated with pronase treatment is a gradual drift in axon activation kinetics. Therefore kinetic stability was monitored throughout our experiments by careful comparison with control records taken before and after each MB^+ application. Kinetic analysis of drug action was attempted only when axon kinetics remained stable.

Series Resistance Compensation

When drug action reduces peak sodium current, any kinetic artifacts arising directly from change in current magnitude must be carefully eliminated before the true kinetics of drug action can be established. Series resistance compensation for 10 $\Omega \cdot cm^2$ produces control axon kinetics that remain unaffected by changes in peak sodium current of comparable magnitude with those induced by MB^+, see Fig. 1. Control axon kinetics remain stable, regardless of whether transmembrane sodium current is reduced by (*a*) changing pore number without altering pore current, as by change of holding potential (see Fig. 1 *A*) or low concentrations of TTX (not shown here), or by (*b*) changing pore current without changing pore number as by lowering external sodium concentration (see Fig. 1 *B*). By contrast, if membrane potential is intentionally shifted by as little as 5 mV (see Fig. 1 *C*) and the currents are then scaled as before, a clear kinetic discrepancy is apparent. Therefore, series resistance errors under these experimental conditions are much <5 mV.

Solutions and Reagents

The compositions of our standard external and internal perfusion solutions are shown in Tables I and II. Low sodium and other solutions were prepared as required by proportionate mixing of these standard solutions. All solutions were checked for pH and osmolarity immediately before use. Clamp conditions were maintained during all solution changes. Solutions

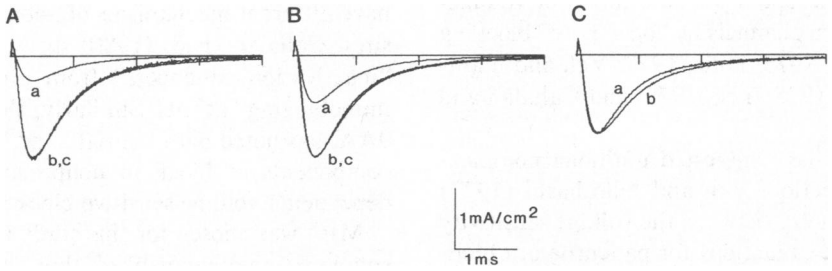

FIGURE 1 Absence of kinetic distortion following reduction in sodium current magnitude. Sodium currents were recorded at 0 mV test potential with series resistance compensation set for 10 $\Omega \cdot cm^2$. Reduction in current magnitude was achieved in *A* by shifting hold potential from −100 to −85 mV and in *B* by lowering external sodium concentration from 50 to 25-mM at a hold potential of −100 mV. Reduced current *a* was scaled in *b* to permit kinetic comparison with the larger current *c*. (*C*) Comparison of sodium current kinetics at 0 mV (*a*) and −5 mV (*b*). Currents scaled to the same peak magnitude to illustrate the amount of kinetic distortion that would be obtained if improper series resistance compensation resulted in an error of 5 mV. *A* and *B*, nonpronased axon 052583, 50 and 25 Na MVH//230 Cs; *C*, nonpronased axon 042583, 50 Na MVH//230 Cs 10 Na.

TABLE I
EXTERNAL SOLUTIONS

Name	Na^+	K^+	Mg^+	Ca^{++}	TMA^+	Cl^-	HEPES	pH
				mM				
NVH*	210	5.4	2.6	13.5	0	247.6	2	7.55
O Na MVH‡	0	0	2.6	13.5	210	242.2	2	7.55
210 Na MVH§	210	0	2.6	13.5	0	242.2	2	7.55

*(NVH) normal Van Harreveld solution (Van Harrveld 1936).
‡(MVH) modified Van Harreveld solution.
§Low external sodium achieved by appropriate mixing of 210 Na MVH with O Na MVH.

TABLE II
INTERNAL SOLUTIONS

Name	K^+	Cs^+	Na^+	TEA^+	TMA^+	F^-	glutamate$^-$	HEPES	pH
					mM				
250 K	250	0	0	0	0	60	190	1	7.35
230 Cs	0	230	0	0	0	60	170	1	7.35
180 Cs 50 Na	0	180	50	0	0	60	170	1	7.35
180 Cs 50 TEA	0	180	0	50	0	60	170	1	7.35
230 TMA	0	0	0	0	230	60	170	1	7.35

All internal and external solutions checked for osmolarity in the range 430–440 mosM.

are listed below as external//internal. All experiments were initiated in 50 Na MVH//250 K, in which the resting potential before clamping was normally −100 to −110 mV. Reagents utilized in this study were methylene blue (Aldrich Chemical Co., Milwaukee, WI), tetrodotoxin (Calbiochem-Behring Corp., American Hoechst Corp., San Diego, CA), tetraethylammonium (Lachat Chemicals, Inc., Mequon, WI), and pronase from *Streptomyces griseus* type VI or XIV (Sigma Chemical Corp., St. Louis, MO), activity: 6 units/mg, or from Calbiochem-Behring Corp., American Hoechst Corp., activity: 77 proteolytic units/mg.

RESULTS

Effects of Internal Methylene Blue on Sodium Current

The effects of two internal MB^+ concentrations (100 and 500 μM) at two different membrane potentials (−20 and +20 mV) before and after pronase treatment are shown in Fig. 2. Several properties of MB^+ block can be readily observed in this figure. (*a*) MB^+ in nonpronased axons (Fig. 2 *A*, *B*) accelerates the decline of sodium current during a step depolarization. This does not reflect a modulation of the normal inactivation process because MB^+ can also induce a falling phase after normal inactivation has been removed by pronase treatment (Fig. 2 *C*, *D*). Therefore MB^+ must act directly on sodium pores, blocking them at a rate that is both concentration and voltage dependent. (*b*) The falling phase kinetics are distinctly different for the pronased and nonpronased conditions. In nonpronased axons the falling phase is faster because it reflects the rates of both drug-induced block and normal inactivation occurring in unblocked pores. (*c*) Although the falling phase is faster in the nonpronased axon, suppression of peak I_{Na} is less marked at both 100 and 500 μM MB^+. This observation suggests that either pronase treatment (or removal of normal inactivation) facilitates MB^+ binding. (*d*) MB^+ has little effect on either the magnitude or kinetics of the early part of the sodium current rising phase. This observation suggests that MB^+ at concentrations of 500 μM or less does not produce

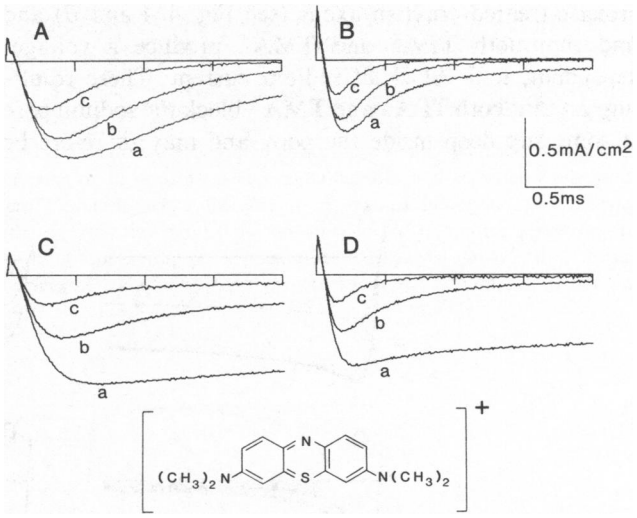

FIGURE 2 Internal MB^+ (see insert) concentration and test potential affect time dependent block of sodium current in both normal and pronase-treated axons. Normal axon at −20 mV (*A*) and at +20 mV (*B*) demonstrates an accelerated decay of I_{Na} in the presence of increasing concentrations of MB^+. Pronased axon shows a simulated inactivation at −20 mV (*C*) and +20 mV (*D*) when internally perfused with MB^+. Each panel contains three superimposed traces: control (*a*) with no drug and with an internal MB^+ concentrations of (*b*) 100 μM and (*c*) 500 μM. Pronased records have been scaled to account for rundown. *A* and *B*, nonpronased axon 042283, 25 Na MVH//230 Cs; *C* and *D*, pronase-treated axon, 031483, 50 Na MVH//230 Cs.

significant block of sodium channels at a holding potential of −100 mV, where nearly all of these channels are in a closed state and might imply that pores must open before MB^+ block can occur. (*e*) MB^+ at concentrations of 500 μM and below has no observable effect on the ON gating current in the absence of external TTX. This can be seen in the unscaled records from the nonpronased axon (Fig. 2 *A*, *B*), where ON gating current is represented by the initial transient outward current at the beginning of each record. This observation also suggests that MB^+ does not interfere with the opening of sodium channels. However, once MB^+ enters a pore, MB^+ can interfere with the closing of both *m* and *h* gates, as will be demonstrated from tail current measurements. (*f*) An increase in MB^+ concentration from 500 μM to 5 mM produces a significant reduction of peak I_{Na} without altering either the falling phase kinetics or time-to-peak (see Fig. 3). This reduction of I_{Na} appears as a tonic rather than time-dependent block. In addition, 5 mM MB^+ reversible suppresses peak I_gON.

Before attempting any detailed kinetic analysis of the MB^+ block, possible interactions between MB^+ and the cations used in the internal perfusates must be carefully considered. Recent evidence has demonstrated that internal cationic substitution of tetramethylammonium (TMA^+) for K^+ can alter the normal gating properties of the sodium channel (Oxford and Yeh 1979; Schauf, 1983). In addition, it has been reported that TMA^+ (Horn et al., 1981) and tetraethylammonium (TEA^+) derivatives (Rojas and Rudy, 1976) can produce voltage-dependent block of the sodium channel. We have looked for these effects in pronase-treated crayfish axons (see Fig. 4 *A* and *B*) and find that both TEA^+ and TMA^+ produce a voltage-dependent, tonic block of sodium current. These results suggest that both TEA^+ and TMA^+ block the sodium pore at some site deep inside the pore, and may therefore be

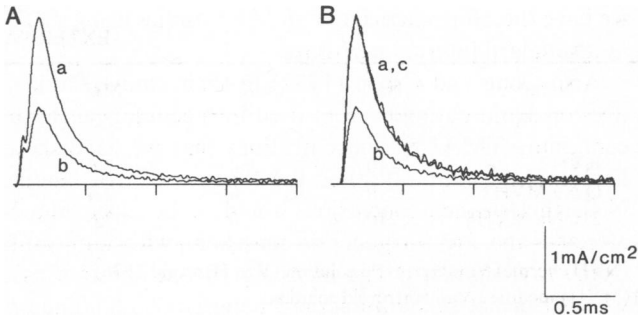

FIGURE 3 Increasing MB^+ concentration from 500 μM to 5 mM at +70 mV suppresses peak I_{Na} without affecting its time-to-peak or falling phase kinetics. Additionally, 5 mM MB^+ reversibly suppresses I_gON. In *A*, a reduction in I_gON and a further reduction of I_{Na} appear as MB^+ concentration is increased from 500 μM (*a*) to 5 mM (*b*). *B* demonstrates that this reduction of I_{Na} occurs without kinetic distortion. After TTX substraction to remove gating and leakage currents, I_{Na} in the presence of 5 mM MB^+ (*b*) is scaled by 2.25 X (*c*) to overly I_{Na} in 500 μM MB^+ (*a*). Pronased axon 072983, 0 Na MVH//180 Cs 50 Na.

expected to interfere or compete with the MB^+ blocking reaction. We have tested for this possibility in Fig. 4 *C* and *D* by comparing the rate of the falling phase of the sodium current in the presence of MB^+ before and after TEA^+ or TMA^+ application. These records demonstrate that changing the internal perfusate either from 230 Cs to 180 Cs, 50 TEA (Fig. 4 *C*) or from 230 Cs to 230 TMA (Fig. 4 *D*) retarded the rate of MB^+ block. This interference with MB^+ block was rapidly reversed by returning to 230 Cs perfusate. By contrast, substitution of internal K^+ with Cs^+ does not produce any observable distortion of either normal sodium current kinetics or the kinetics of MB^+ block (not shown). Internal cationic substitution with Cs^+ eliminates potassium currents, greatly reduces leakage current, and also prevents any distortion of MB^+ kinetics;

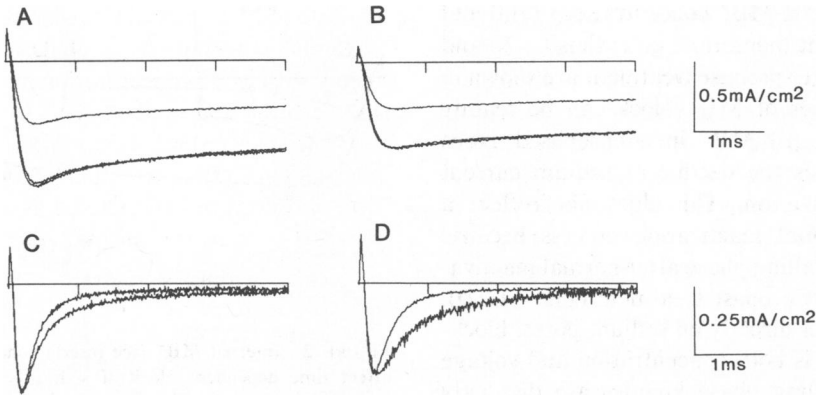

FIGURE 4 TEA^+ and TMA^+ block sodium pores and affect the rate of I_{Na} block produced by 500 μM MB^+ in pronased axons. Sodium currents measured at 0 mV with Cs^+ as the major internal cation demonstrate that (*A*) addition of 50 mM TEA to the Cs^+ perfusate and (*B*) substitution of Cs^+ with TMA^+ both produced a constant suppression of I_{Na} by 49 and 46%, respectively. Reduced currents kinetically superimpose control currents when scaled to equal peak magnitude. The addition of 500 μM MB^+ to 230 Cs internal perfusate produces a time-dependent block of I_{Na} (in pronased axons). The kinetics of MB^+ block are retarded in *C* by switching to 180 Cs 50 Na and in *D* by substitution of 230 Cs with 230 TMA. Traces scaled to equal peak magnitude to facilitate kinetic comparison of MB^+ blocking rate. Gating currents were blanked in the scaled records. *A*, pronased axon 042783, 50 Na MVH//230 Cs and 180 Cs 50 TEA; *C*, pronased axon 041283, 100 Na MVH//230 Cs and 180 Cs 50 TEA; *B* and *D*, pronased axon 052783, 50 Na MVH//230 Cs and 230 TMA.

we have therefore carried out all MB^+ studies using 230 Cs as a standard internal perfusate.

Armstrong and Croop (1982) in their study of thiazin dyes on squid gating current used intracellular perfusates containing TMA^+ in concentrations that we have shown here can substantially alter the kinetics of dye binding. Nevertheless, their conclusions would not be expected to be affected and are, in general, consistent with our results from crayfish axons. The more significant question as to whether or not such interactions between dye binding and quarternary ammonium ion binding involve competition for the same receptor site, remains unresolved in the present study.

Effects of MB^+ on Sodium Tail Currents

The effect of MB^+ on sodium tail currents in nonpronased axons is shown in Fig. 5. A comparison is made from the same axon with control tail currents (Fig. 5 *A*) and with tail currents in the presence of 500 μM MB^+ (Fig. 5 *B*). MB^+ produces a "hooked" tail current apparently resulting from the relatively slow dissociation of bound drug and an interference by bound drug with the closure of *m* gates, as first suggested by Yeh and Narahashi (1977) for pancuronium. Notice that the shape of the MB^+ tail current changes as MB^+ block develops progressively with increasing pulse duration at test potential (Fig. 5 *B*). MB^+ tail current kinetics following a 0.1 ms test pulse appear identical to control tail current kinetics. However, as test pulse duration is increased from 0.1 to 2 ms, the shape of the tail current changes. This results from the summed effects of two pore populations: unoccupied pores showing normal, fast tail-current kinetics and drug-bound pores showing slowed tail-current kinetics. With increasing test pulse duration, the progressive loss of the sharp early tail-current spike and the increase in slow kinetics parallels the inactivation of normal unblocked pores and an increase in the number of MB^+ blocked pores. At pulse durations longer than 2 ms, after steady state block has been achieved, the shape of the tail current remains unchanged.

In normal axons (Fig. 5 *A*), change in tail-current magnitude parallels the rate of normal inactivation, thus tail-current magnitude continues to decrease with increasing test pulse durations. However, in the presence of MB^+, there is little loss of tail-current magnitude at comparable

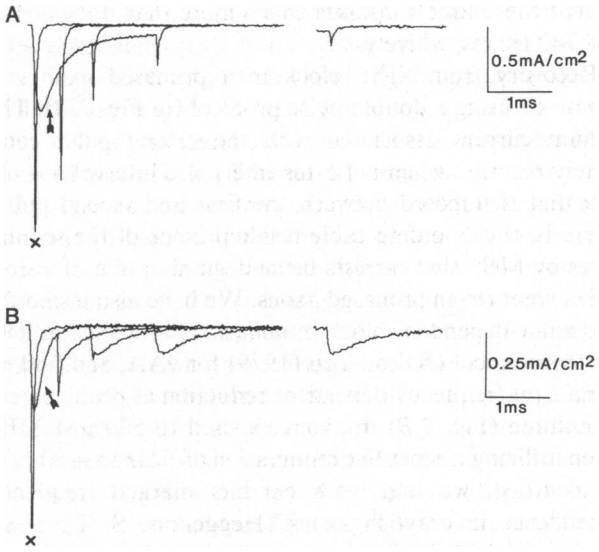

FIGURE 5 MB^+ effects both the magnitude and kinetics of sodium tail currents in nonpronased axons. This figure shows (*A*) control tail currents and (*B*) hooked tail currents in the presence of 500 μM MB^+. Tail currents were recorded at a hold potential of −100 mV following varying test pusles to +40 mV. Pulse durations at +40 mV were 0.1, 0.5, 1, 2, and 8 ms. Gating currents have been subtracted using comparable records collected in zero external sodium. Sodium current associated with test potential is identified with an arrow (↑) so as to distinguish it from adjacent tail current traces. The peak tail currents are off scale in traces labeled with (X). *A* and *B*, nonpronased axon 052583, 50 Na MVH//230 Cs.

durations (Fig. 5 *B*). A further increase in test pulse duration to 32 ms (not shown) does not significantly reduce the magnitude of hooked-tail currents. This observation suggests that MB^+ can interfere with, or protect the channel from normal inactivation and that the *h* gate cannot close while a pore is occupied by MB^+.

The rate of MB^+ block was shown in Fig. 2 to be both concentration and voltage dependent. However, the apparent rate of MB^+ dissociation (as observed from hooked tail currents) is voltage dependent, but does not vary appreciably with MB^+ concentration in the range 50 to 500 μM. Fig. 6 shows MB^+ tail currents in the presence of 500 μM MB^+ from a pronased axon returning to −120 mV (*A*) and −80 mV (*B*) with calculated tail-current falling phase time constants of 216 and 888 μs, respectively. Decreasing the MB^+ concentration by a factor of five (to 100 μM)

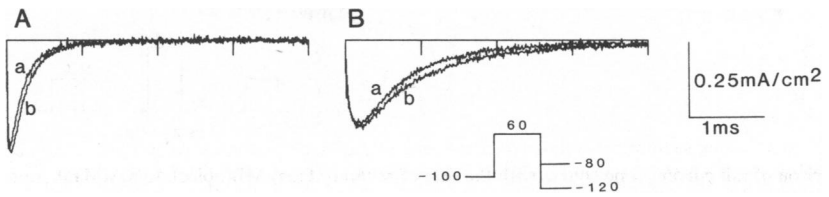

FIGURE 6 The kinetics of MB^+ tail currents are voltage dependent but not markedly concentration dependent for a fivefold change in MB^+ concentration, 100 μM (*a*) to 500 μM (*b*). Tail currents were generated, following a 5-ms test pulse to +60 mV, by step repolarization to −120 mV (*A*) and −80 mV (*B*). In *A*, increasing the MB^+ concentration from 100 to 500 μM changed the falling phase time constant from 198 μs to 216 μs for tail currents at −120 mV. In *B*, this increase in MB^+ concentration changed the tail current time constant at −80 mV from 742 to 888 μs. *A* and *B*, pronased axon 060283, 100 Na MVH//230 Cs.

altered these time constants by no more than 17% to 198 and 742 μs, respectively.

Recovery from MB^+ block in a pronased axon was examined using a double-pulse protocol (in Fig. 7 *A*). The sodium current associated with the second pulse completely recovers when a 1.5-ms interpulse interval at hold potential is imposed between the first and second pulse. There is, thus, no detectable residual block of the sodium pores by MB^+ that persists beyond the duration of visible tail current (*a*) in pronased axons. We have also tested for frequency-dependent block in nonpronased axons, following the protocol used by Yeh (1979) for 9AA, and find no significant frequency-dependent reduction of peak current magnitude (Fig. 7 *B*) in axons exposed to 500 μM MB^+ when utilizing a repetitive stimulation of 1 Hz to +50 mV. By contrast, we find 9AA exhibits marked frequency dependence in crayfish axons (Heggeness, S. T., J. G. Starkus, and M. D. Rayner, unpublished observations) as seen in squid axons (Cahalan, 1978; Yeh, 1979).

Tail-current magnitudes have previously been used to provide an estimate of the relative numbers of sodium channels open at the time of peak conductance at different test potentials (Dodge and Frankenhaeuser, 1959; Woodhull, 1973). We have adapted this method to assess the fraction of channels blocked by MB^+, by measuring the relative magnitudes of the hooked-tail currents developed on return to holding potential from different test potentials (after careful subtraction of any fast-kinetic tail-current component generated in unblocked pores, see Armstrong and Croop, 1982). Thus, in Fig. 8 *A*, we see nearly identical tail currents on return from a 6-ms pulse to either +40 or O mV. Presumably at both these test potentials 500 μM MB^+ blocks essentially all available pores within 6 ms. By contrast, the tail current following a 6-ms pulse to −40 mV is only ~60% of the magnitude of the +40-mV record, suggesting that only some 60% of sodium pores are blocked

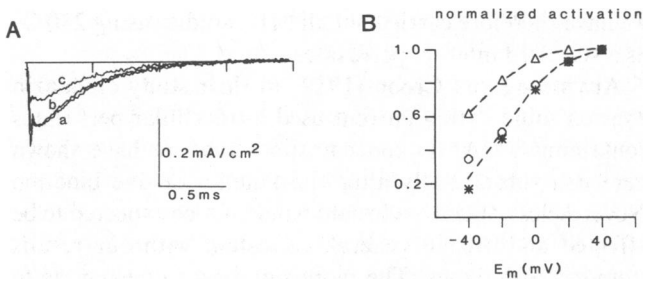

FIGURE 8 (*A*) Hooked sodium tail currents at −100 mV in the presence of 500 μM MB^+ following 6-ms depolarization to three different test potentials. Tail currents are nearly identical following test depolarizations to +40 mV (*a*) and 0 mV (*b*), but are reduced by 40% upon repolarization from −40 mV test potential (*c*). These hooked tail currents are kinetically identical following subtraction of the fast tail current component generated from normal unblocked sodium channels (see text). (*B*) Compares the normalized fraction of sodium channels associated in hooked tail currents with two estimates of sodium channel activation in the voltage range −40 to +40 mV. The estimate of drug blocked open channels (Δ) in the presence of MB^+ are consistently greater than either Q_{ON}/Q_{ON} max (○) or G_{Na}/G_{Na} max (*) estimates of open channels under control conditions, dashed lines drawn by eye. Results indicate that more sodium channels are gated open in the presence of MB^+ than in comparable control records from the same axon. Pronased axon 052783, 50 Na MVH//230 Cs.

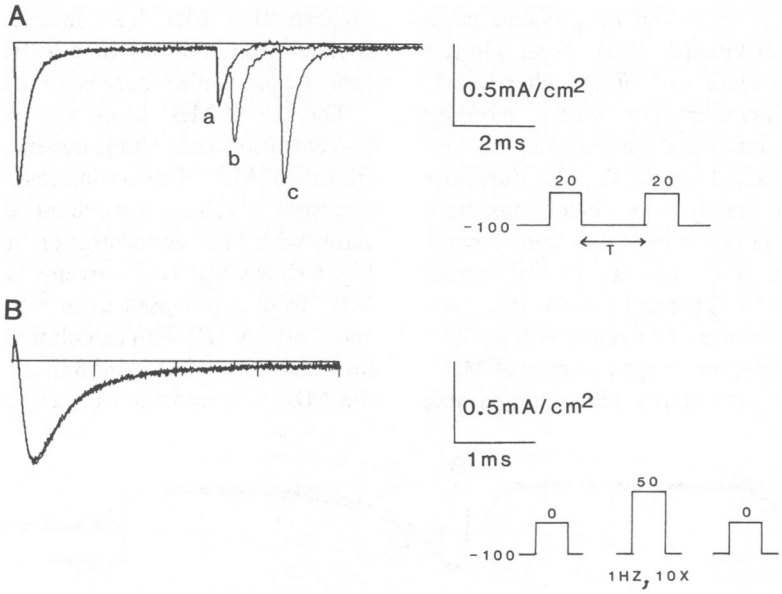

FIGURE 7 (*A*) Comparison of tail current time course with the rate of recovery from MB^+ block (500 μM) in a pronased axon. When tail current (*a*) is complete and decays to zero baseline, I_{Na} shows complete recovery. Measurements of I_{Na} recovery obtained by a double pulse protocol (to +20 mV) with variable interpulse intervals (*T*) at hold potential (−100 mV). Partial recovery (65%) occurs with an interpulse interval of 300 μs (*b*). Complete recovery occurs with a 1.5-ms interpulse interval (*c*). (*B*) Absence of frequency dependent block in nonpronased axon perfused with 500 μM MB^+. Two superimposed traces show sodium current before and immediately after 10 conditioning pulses to +50 mV at 1 Hz. No frequency dependent reduction in current magnitude can be observed. *A*, pronased axon 061883, 100 Na MVH//230 Cs. *B*, nonpronased axon 101382, 50 Na MVH//230 Cs.

by MB^+ under these conditions. This figure is, however, several fold higher than the fraction of sodium pores that might have been expected to be activated at that potential under control conditions (see Fig. 8 *B*). Estimates derived from measurements of both peak sodium conductance and gating charge movement from the same axon in absence of MB^+ would suggest only some 20% of sodium pores are normally activated at −40 mV. The implication that MB^+ may increase the fraction of sodium pores activated when m_∞ is <1.0, will be considered further in the Discussion section.

Quantitative Description of MB^+ Block

The qualitative data provided above seem sufficient to indicate the major features of MB^+ action in crayfish axons. Internally applied methylene blue appears to block sodium pores in a voltage and time-dependent manner and in such a way as to prevent closure of either *m* or *h* gates, while MB^+ remains bound to its receptor site.

Two methods are available for quantitative description of time-dependent channel block, as noted by French and Shoukimas (1981). In the first method, a single exponential is fitted to the drug-induced falling phase, while in the second, drug action is calculated from a plot of the ratio $I_{drug}/I_{control}$. In the present paper, this second method has been modified to produce a percent difference plot. This plot is calculated as $100(I_{control}-I_{drug})/I_{control}$, to facilitate a graphic presentation of apparent blocking rate. Clearly these two methods, the falling phase method and the percent difference method, should give identical results when the drug effect is measured over a period of time where I_{Na} is constant in the control record. However, the falling phase method may well be expected to give unreliable results both where there is any lingering inactivation in the pronase-treated control record and/or where the time constant of the drug effect approaches the activation rate of control sodium current.

These two analytical methods are compared in Fig. 9. Trace *a* shows the control record for this pronased axon, obtained after washout of MB^+, while trace *b* is the experimental record obtained in presence of 500 μM MB^+.

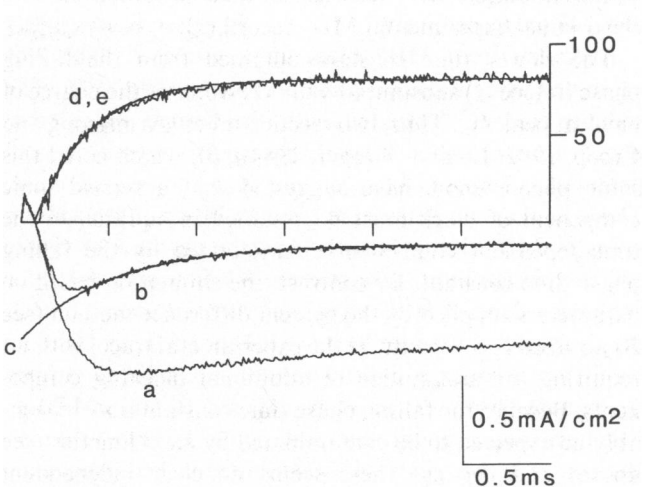

FIGURE 9 Analysis of MB^+ blocking kinetics by the falling phase method and the percent difference method yield different results. At −20 mV, control I_{Na} is shown as *a*, and *b* shows I_{Na} in presence of 500 μM MB^+. The rate of MB^+ block can be estimated directly from the falling phase of I_{Na} in *b*, which yields a time constant of 515 μs and a steady state block of $p = 81\%$. Trace *c* shows a single exponential with time constant of 515 μs fitted to the falling phase of I_{Na}. Alternatively the rate of MB^+ block can be estimated using the percent difference technique (*d*). This trace yields a time constant of 306 μs and a steady state block of $p = 81\%$. Trace *e*, smooth curve, shows a single exponential with these parameters fitted to the percent difference curve. Pronased axon 121582, 50 Na MVH//230 Cs.

The falling phase of this record was fitted by a least-squares method to a single exponential and an excellent fit (trace *c*) was obtained with a time constant of 515 μs. The percent difference record, obtained after TTX subtraction for removal of gating and leakage currents, is shown as trace *d* of this figure. This trace was also fitted by a least-squares method to obtain a single exponential (trace *e*) but this time yielding a faster time constant of 306 μs. Both analyses indicate identical values for equilibrium block (81%).

In Fig. 10 we compare the utility of these estimates as quantitative descriptors of the MB^+ effect. In each panel, a calculated single exponential is subtracted from the control record (*a*) and displayed as a simulated MB^+ record (*b*).

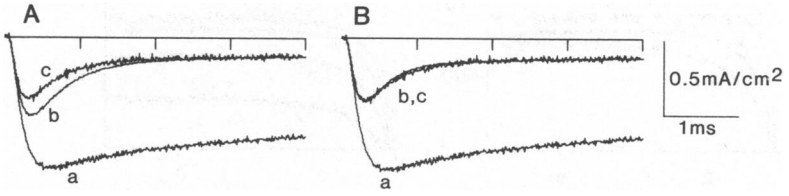

FIGURE 10 Comparison between experimental record at −20 mV in the presence of 500 μM MB^+ and traces simulated from the two analytical methods illustrated in Fig. 9. For each panel, the calculated rate of block was subtracted from the control record (*a*) on a point by point basis. These simulated MB^+ records (*b*) obtained for each analytical method can be compared with the experimental MB^+ record (*c*). In *A* the parameters obtained from the falling phase method ($\tau_{MB} = 515$ μs and $p = 81\%$) do not accurately simulate the experimental record and underestimate the degree of block at peak I_{Na}. By contrast, in *B*, the parameters obtained from the percent difference method ($\tau_{MB} = 306$ μs and $p = 81\%$) present an accurate simulation of the experimental record. Traces *a* and *c* were plotted from Fig. 9 following TTX subtraction to remove gating and leakage currents.

These simulated MB^+ records can then be compared with the original experimental MB^+ record (*c*).

The slower time constant obtained from the falling phase fit (see *A*) substantially underestimates the degree of block at peak I_{Na}. Thus, two recent studies (Armstrong and Croop, 1982; Lo and Shrager, 1981*a*, *b*), which noted this same phenomenon, have suggested that a second tonic component of block must be assumed in addition to the time-dependent component characterized by the falling phase time constant. By contrast, the simulation based on parameters supplied by the percent difference method (see *B*) accurately reconstitutes the experimental trace, without requiring the assumption of additional blocking components. Because the falling phase time constant may reasonably be expected to be contaminated by axon kinetics (see above) and because there seems no clear independent evidence for the existence of more than one component of block by MB^+, we have chosen to use the percent difference method for quantitative description of MB^+ effects throughout the remainder of this study.

Kinetics of MB^+ Action

The concentration and voltage dependence of the observed MB^+ action is illustrated in Fig. 11 using the percent difference method. The concentration dependence of this effect is shown in Fig. 11 *A*. At constant test potential (0 mV) increasing MB^+ concentration from 50 to 500 μM increases both the rate of block and the level of block reached at equilibrium. Fig. 11 *B* shows the voltage dependence of the MB^+ effect. At constant MB^+ concentration (100 μM) a block is both more rapid and complete at positive test potentials. This figure also reveals a short voltage-sensitive delay period before the visible onset of MB^+ block. This delay decreases from 180 μs at -40 mV to 60 μs at $+20$ mV. Because the MB^+ block is not visible until pores are open, most of this delay presumably reflects a voltage-dependent initial delay in sodium pore opening (Starkus et al., 1981) similar to that seen in squid axons by Keynes and Rojas (1976).

Time constants for the blocking reaction (τ_{MB}) were calculated from the percent difference plots by a least-squares fit to a single exponential. Excellent fits were normally obtained, although a small slower component was visible in some records, in particular those at higher drug concentrations and positive potentials. This slow component has been ignored in our preliminary analysis since its time-zero intercept was always <5% of the fast component intercept. The time constants evaluated from the percent difference analysis are summarized in Table III. The blocking time constants are highly concentration dependent in the range 50 to 500 μM, but this concentration dependence falls off above 500 μM. Results from one experiment using 5 mM MB^+ on outward sodium currents (see Table II) reveal little additional acceleration of τ_{MB} for a further 10-fold increase in MB^+ concentration. The voltage dependence of the blocking reaction is most clearly evident at 100 and 500 μM MB^+. At these concentrations, a steep voltage dependence is observed in the negative potential range, approaching a concentration-dependent asymptote at positive potentials.

Table IV summarizes the equilibrium block (*p*) values obtained at these same MB^+ concentrations. Equilibrium block is also concentration and voltage dependent. Again a steep voltage dependence is observed in the negative potential range at all three MB^+ concentrations. The equilibrium values and time constants obtained for MB^+ block show small but consistent differences between values obtained from inward and outward sodium currents (see Table II and III). For inward sodium currents, the sodium concentrations were primarily 50 mM on the outside and O mM on the inside, while for outward sodium current the sodium gradient was identical but reversed in direction.

Descriptive parameters obtained using either the falling phase or percent difference methods can provide a quantitative estimate of the kinetics of MB^+ binding only where such binding occurs independently of channel state; in other words, where the drug binds with equal affinity to the resting, open, and inactivated states of the sodium channel. Where binding occurs preferentially to any particular

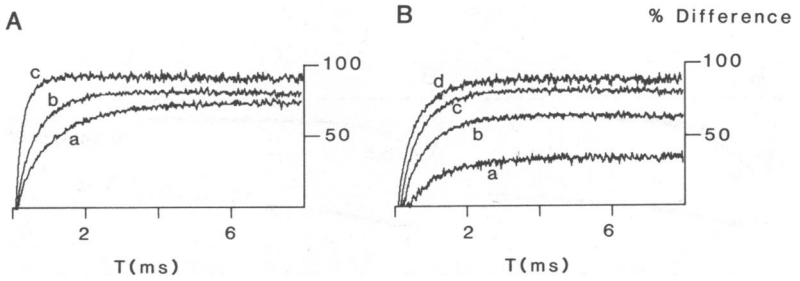

FIGURE 11 The rates of MB^+ block show both concentration and voltage dependence in pronased axons. (*A*) Comparison of the kinetics of block at 0 mV using three concentrations of MB^+: (*a*) 50 μM, (*b*) 100 μM, and (*c*) 500 μM. Increasing concentrations of MB^+ accelerate the rate of MB^+ block and increase equilibrium block. (*B*) Voltage dependence of block by 100 μM MB^+: (*a*) -40 mV, (*b*) -20 mV, (*c*) 0 mV, (*d*) $+20$ mV. With increasing step depolarization, the rate of MB^+ block is accelerated and equilibrium block is increased. *A*, pronased axon 031583, 50 Na MVH//230 Cs + 50 μM MB^+, pronased axon 122382 50 Na MVH//230 Cs + 100 μM MB^+, pronased axon 031483 50 Na MVH//230 Cs + 500 μM MB^+. *B*, pronased axon 122382 50 Na MVH//230 Cs + 100 μM MB^+.

TABLE III
TIME CONSTANTS FROM THE PERCENT DIFFERENCE FOR INWARD AND OUTWARD SODIUM CURRENTS

E_m	50 μM MB^+		100 μM MB^+		500 μM MB^+		5 mM MB^+
	Inward	Outward	Inward	Outward	Inward	Outward	Outward
mV	*μs*	*μs*	*μs*	*μs*	*μs*	*μs*	*μs*
−40	748 ± 50(2)	—	702 ± 58(6)	—	400 ± 37(9)	—	—
−30	826 ± 49(2)	—	662 ± 60(3)	—	359 (1)	—	—
−20	873 ± 31(3)	—	647 ± 41(6)	—	281 ± 31(9)	—	—
−10	858 ± 49(2)	—	584 ± 30(3)	—	238 ± 24(3)	—	—
0	879 ± 6(3)	854 ± 48(3)	561 ± 38(6)	497 ± 33(3)	197 ± 8(9)	160 ± 25(3)	—
+10	873 ± 23(3)	845 ± 72(3)	503 ± 38(3)	496 ± 45(3)	169 ± 7(4)	130 ± 23(4)	113(1)
+20	837 ± 30(3)	797 ± 102(3)	498 ± 37(6)	447 ± 44(3)	155 ± 7(9)	119 ± 16(4)	84(1)
+30	810 ± 33(3)	786 ± 85(3)	462 ± 26(3)	427 ± 21(3)	144 ± 8(5)	109 ± 14(4)	79(1)
+40	—	783 ± 77(3)	—	421 ± 13(3)	—	104 ± 13(4)	77(1)
+50	—	773 ± 73(3)	—	418 ± 18(3)	—	98 ± 11(4)	74(1)
+60	—	813 ± 33(2)	—	416 (1)	—	95 ± 10(4)	70(1)
+70	—	771 ± 61(3)	—	410 ± 12(3)	—	95 ± 14(4)	62(1)
+80	—	787 ± 59(2)	—	393 (1)	—	91 ± 14(4)	58(1)
+90	—	762 ± 68(3)	—	408 ± 28(3)	—	85 ± 6(4)	55(1)

channel state, occupancy of that state will necessarily be altered by comparison with control conditions. Thus, both the transition rates and equilibria for all preceding and subsequent reaction steps will also be materially affected by the drug-binding process (see Discussion). Thus, not only will τ_{MB} values be distorted, but p values also may be quite different from the true equilibrium of the binding reaction.

In the following paragraphs we will pursue a standard analysis of the kinetics of the MB^+ binding as if this process were a state-independent pseudo–first-order reaction. Quantitative presentation of our data in this form provides for direct comparisons with results of other studies that have utilized a similar analytical method, and serves to confirm the kinetic anomalies seen by other workers.

Presuming that only a single energy barrier limits access of MB^+ to its binding site and that the binding reaction follows pseudo–first-order kinetics, the apparent rate constants for the forward and backward reactions, k (kappa) and l (lambda) respectively, can be calculated from our mean values of τ_{MB} and equilibrium block (p) as

$$k = p/\tau_{MB} \quad (1)$$

$$l = (1 - p)/\tau_{MB}. \quad (2)$$

Results of this analysis are presented graphically in Fig.

TABLE IV
EQUILIBRIUM BLOCK (p) OF INWARD AND OUTWARD SODIUM CURRENTS BY MB^+

E_m	50 μM MB^+		100 μM MB^+		500 μM MB^+		5 mM MB^+
	Inward	Outward	Inward	Outward	Inward	Outward	Outward
mV	%	%	%	%	%	%	%
−40	20 ± 3(2)	—	41 ± 6(6)	—	71 ± 7(9)	—	—
−30	34 ± 2(2)	—	58 ± 4(3)	—	79 (1)	—	—
−20	48 ± 3(3)	—	67 ± 5(6)	—	89 ± 4(9)	—	—
−10	59 ± 1(2)	—	79 ± 2(3)	—	95 ± 3(3)	—	—
0	73 ± 1(3)	81 ± 6(3)	85 ± 2(6)	91 ± 3(3)	95 ± 2(9)	95 ± 2(3)	—
+10	80 ± 2(3)	89 ± 3(3)	89 ± 2(3)	93 ± 2(3)	98 ± 2(4)	96 ± 2(4)	98(1)
+20	84 ± 4(3)	92 ± 2(3)	92 ± 1(6)	96 ± 1(3)	97 ± 2(9)	97 ± 2(4)	97(1)
+30	88 ± 2(3)	95 ± 1(3)	93 ± 2(3)	97 ± 1(3)	98 ± 1(5)	98 ± 1(4)	98(1)
+40	—	96 ± 1(3)	—	98 ± 1(3)	—	99 ± 1(4)	98(1)
+50	—	97 ± 1(3)	—	99 ± 0(3)	—	100 ± 1(4)	98(1)
+60	—	98 ± 0(2)	—	99 (1)	—	100 ± 1(4)	98(1)
+70	—	99 ± 1(3)	—	100 ± 0(3)	—	100 ± 1(4)	98(1)
+80	—	100 ± 1(2)	—	100 (1)	—	100 ± 1(4)	99(1)
+90	—	100 ± 0(3)	—	100 ± 0(3)	—	100 ± 1(4)	99(1)

Data are given as mean ± SD (n equals the number of axons). Inward currents obtained with 50 Na MVH//230 Cs. Outward currents obtained with 0 Na MVH//180 Cs 50 Na.

12. Fig. 12 *A* shows the effects of test potential and MB^+ concentration on the forward rate constant, calculated by Eq. 1. The effect of MB^+ concentration is apparent in that a doubling of MB^+ concentration from 50 to 100 μM accelerates k by two-fold across the entire voltage range. However, the fivefold increase from 100 to 500 μM MB^+ produces a four to fivefold acceleration of k at positive test potentials, but only a threefold acceleration of k at negative voltages, as if the concentration effect is beginning to saturate at 500 μM MB^+ at negative potentials. The voltage sensitivity of the forward rate constant is also clearly demonstrated in Fig. 12 *A*. It is apparent that k is markedly more voltage sensitive in the negative potential range than at positive potentials. The reduced voltage sensitivity of MB^+ binding at positive potentials is also evident in the τ_{MB} data of Table II. τ_{MB} changes little with voltage at positive potentials although it remains dependent on MB^+ concentrations.

Fig. 12 *B* demonstrates the effects of test potential and MB^+ concentration on the backward rate constant calculated using eq. 2. This rate constant seems essentially independent of MB^+ concentration and, in contrast to the forward rate constant, shows linear voltage sensitivity on a semilog plot.

The predicted voltage sensitivity of a pseudo–first-order reaction between a charged site within the transmembrane voltage field and a nonpermeant MB^+ ion can be expressed by the following rate equations (Glasstone et al., 1941; Woodhull, 1973; Yeh and Narahashi, 1977)

$$k = ([MB]/K_D)A \exp(dxEzF/RT) \quad (3)$$

$$l = A \exp(-d(1 - x)EzF/RT). \quad (4)$$

Here A is a proportionality factor (expressed in μs^{-1}) that includes both the conventional collision frequency factor and the average barrier height, while K_D is the concentration of MB^+ yielding 50% equilibrium block at 0 mV. The remaining terms define the effect of membrane potential on these rate constants: d (delta) is the fraction of the voltage field crossed when MB^+ reaches its binding site from the internal perfusate, x is a symmetry factor defining barrier position, E is the applied transmembrane potential, z is the valence of MB^+ (here assumed to be +1) and F, R, and T have their usual meanings. Note that where K_D is defined as above, any difference in energy levels between the two reaction wells at 0 mV will affect the apparent value of K_D.

This model could be fitted to our data in either of two ways. One could assume symmetrical voltage sensitivities in both forward and back reactions, and fit the values of k seen between −40 and 0 mV. This approach yields a value for delta of ~1.6 (where $x = 0.5$), a value too high to be consistent with a first-order representation of this reaction. Alternatively, the rate constants can be presumed asymmetric (as also noted by Yeh and Narahashi, 1977). When k is fitted only to data between +30 and +90 mV, a more reasonable fit is obtained yielding $d = 0.85$ (where $x = 0.03$).

The forward rate constants predicted by the asymmetric first-order model fit the data of Fig. 12 *A* reasonably well at positive potentials (from +30 to +90 mV) and at the lower two MB^+ concentrations (50 and 100 μM). The predictions of this pseudo–first-order model deviate markedly from the observed forward rate constants between 0 and −40 mV at these concentrations, and for 500 μM

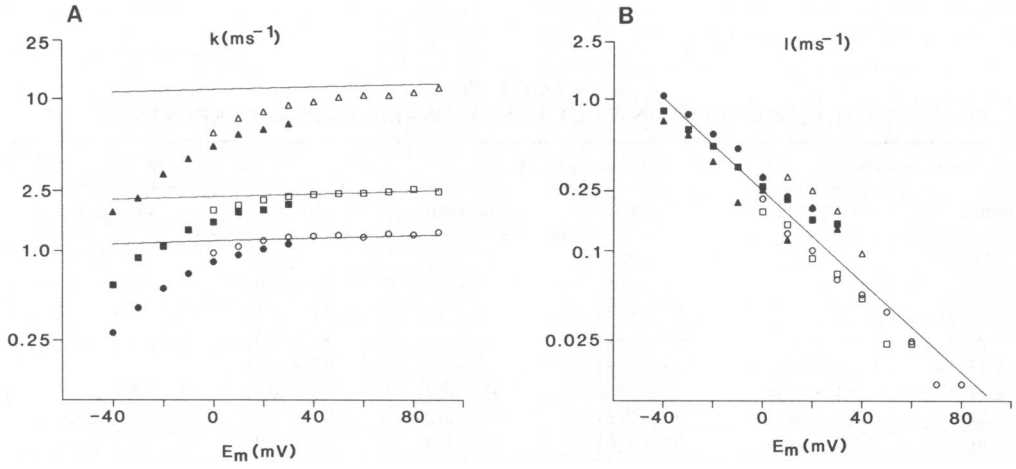

FIGURE 12 Effect of membrane potential on the apparent forward rate constant (k) and the apparent backward rate constant (l), as calculated from Eqs. 1 and 2. (*A*) k is steeply voltage dependent at negative membrane potentials and less voltage dependent at positive potentials. k is also concentration dependent, increasing as MB^+ concentration is increased from 50 μM (○) to 100 μM (□) to 500 μM (△). Solid symbols (▲, ■, ●) calculated from inward I_{Na} (50 Na MVH//230 Cs) and open symbols (△, □, ○) calculated from outward I_{Na} (0 Na MVH//180 Cs 50 Na). The solid line fits were obtained from Eq. 3 (K_D = 11 μM MB^+, d = 0.85, x = 0.03, A = 0.25 ms^{-1}) and demonstrate a poor fit by the pseudo–first-order model at negative membrane potentials and for 500 μM MB^+ at all test potentials. (*B*) l is steeply voltage dependent at both positive and negative membrane potentials, but is relatively independent of MB^+ concentration. The solid line fit was obtained from Eq. 4 (d = 0.85, [1 − x] = 0.97, A = 0.25 ms^{-1}) describing the pseudo–first-order model. Data points calculated from Table III and IV.

MB^+ at all but the most positive test potentials. The backward rate constants predicted by this model (solid line) are a good fit to the data presented in fig. 12 *B* at all membrane potentials.

Quantitative analysis of our results thus serves to confirm the similarity between the kinetics of MB^+ block and the kinetics of block observed with other open-pore blocking agents. (*a*) At positive potentials the calculated forward and backward rate constants show markedly asymmetric voltage sensitivity. (*b*) The calculated forward rate constant appears voltage sensitive at negative potentials. This phenomenon was also noted for pancuronium by Yeh and Narahashi (1977). (*c*) Only the forward reaction rate is affected by MB^+ concentrations. (*d*) The increase in blocking rate, associated with increasing drug concentration, saturates at concentrations in the millimoles per liter range. Thus, Yeh and Narahashi (1977, Fig. 12 *A*) show only a fivefold change in the forward rate constant for a tenfold increase in pancuronium concentration (100 μM to 1 mM). This effect has been investigated in more detail by Lo and Shrager (1981 *a*,*b*) for a *n*-propyl guanidinium binding at positive potentials, and has been shown to be inconsistent with any simple first-order model. (*e*) Finally, MB^+, like pancuronium, shows little difference in the degree of block for inward or outward currents. Thus, Yeh and Narahashi (1977) noted no consistent effect of current direction in their kinetic analysis of pancuronium block. In Fig. 12 note that k is slightly increased and l reduced for outward sodium currents. These shifts are not readily compatible with any simple change of K_D or change in barrier height; such changes would not move both rate constants in opposite directions. We note that our observed results could be explained by a 10-mV shift along the voltage axis and that the effect is very small compared with the sharp effects of internal sodium concentration on open pore block by *N*-alkylguanidinium derivatives (Lo and Shrager, 1981*a*,*b*; Smith et al., 1983). The appropriateness of this analytical approach, as well as the implications of these results with respect to the nature of the MB^+ binding reaction, must now be considered.

DISCUSSION

Na Pore Block by MB^+

Dyes of the methylene blue, azure A, series have also been studied recently by Armstrong and Croop (1982) using internally perfused squid axons. The results we have presented here seem in excellent qualitative agreement with their work. Both studies demonstrate that at micromolar concentratins, such dyes show little binding at negative holding potentials (in absence of external TTX) and that they block sodium pores directly, rather than by enhancing the rate of the normal inactivation process. The binding site for the dye molecule must be such that the dye-blocked state prevents closure of either activation or inactivation gates. From these observations methylene blue can be categorized with "gate immobilizing" open-pore blockers (Cahalan et al., 1980) rather than being an "inactivation enhancer."

The evidence that suggests that these agents block in a strictly state-dependent, open-pore manner is qualitative, and is not conclusive. The appearance of hooked tail currents indicates that drug-blocked open channels cannot close until after the drug has dissociated from its receptor. If this interference with *m*-gate closure is due to a physical blockade of the *m*-gate (Yeh and Narahashi, 1977), then a closed *m*-gate would presumably prevent access of the drug to its binding site, and block would necessarily be state dependent. There are, however, alternative explanations for the appearance of hooked tail currents and MB^+ binding may not necessarily be strictly state dependent. For example, steric or electrostatc interactions from a drug binding site axoplasmic to the *m*-gate could modify the probability of *m*-gate closure. Drug access to such a site need not be prevented by a closed *m*-gate, although binding site affinity may well be affected by *m*-gate position. In an effort to further evaluate the nature of the MB^+ binding reaction, we explore the properties of both state-dependent and state-independent blocking schemes in the following section.

Mechanisms of Time-dependent Block

Time-dependent block of sodium channels by MB^+ can be discussed, in pronased axons, by reference to the following simplified reaction scheme:

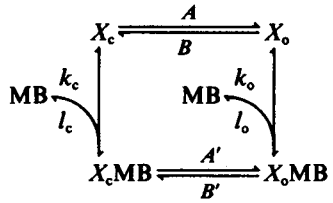

Scheme I

in which X_c represents all pre-open states and X_o represents the open and conducting state(s). MB^+ block can be considered fully state independent only when the rate constants l_c, k_c, A, and B are indistinguishable from l_o, k_o, A', and B'. If these conditions are not met, MB^+ binding will be either partially or fully state dependent, depending on the magnitude of the differences between these two groups of rate constants.

State-independent Block. In this form of block the blocking agent acts similarly to a Hodgkin-Huxley *h*-gate and a drug block would not be expected to alter either the equilibrium values or transition rates between states X_c and X_0. Thus the percent difference records would accurately reflect the kinetics of the drug-blocking reaction. However, this model does not require simple exponential voltage dependence of k and l. It remains possible that MB^+ could block the sodium pore by binding to one of a sequence of sites normally involved in sodium ion perme-

ation. If this were the case, voltage-dependent changes in the occupancy of one ion binding site might affect the availability or affinity of another site, the drug binding site. In this way, the apparent valence of the blocking reaction could be both greater than one and test potential dependent. If the sodium permeation channel of crayfish axon is in fact multi-ion in behavior, this could explain the anomalous voltage sensitivity observed in Fig. 12 and also offer a possible explanation for the small observed differences between the effects of MB^+ on inward and outward I_{Na}.

State-dependent Block. If drug block occurs exclusively, or even predominantly, from a specific state (or states), then the development of block will necessarily alter the kinetics of channel gating. In the following simplified example of open-pore block

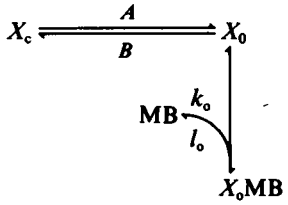

Scheme II

it is clear that, as open channels (X_o) are converted to the drug-blocked state (X_oMB), the equilibrium of the X_c to X_0 transition will be shifted to the right by mass action (see Appendix). This product trapping phenomenon will effectively pull channels from state X_c through state X_o into state X_oMB. Thus the apparent τ_{MB}, obtained by either the percent difference or falling phase methods, would be distorted by the altered kinetics of the X_c to X_o transition. Similarly, p will be affected not only by drug block but also by the shift of the X_c to X_o equilibrium away from its control value. Both of these effects would be expected to be maximal at negative test potentials, where activation is slow and incomplete, and minimal at positive test potentials where equilibrium occupancy of the X_o state(s) will be close to 1.0 in the control records. This explanation has been invoked by Coronado and Miller (1979) to account for the differences between macroscopic and single channel approximations of the Cs^+ binding constant for K^+ channels in sarcoplasmic reticulum.

An obvious property of the simple sequential reaction scheme described above is that the observed rate of MB^+ action should show multiple exponential components. However, the extent to which such multiple exponentials might be discernible within the apparent blocking rate is dependent on both the number of pre-open states assumed and the individual rate constants chosen for each closed state transition. The situation becomes even more complex in partially state-dependent block (such as could be modeled by a Scheme I in which l_c, k_c, A, and B are not equal to l_o, k_o, A', and B'). Our preliminary evaluation of such models suggests that close approximations to single exponential blocking rates are often obtained from partially or fully sequential systems, although in these schemes the observed rate of block (τ_{MB}) may show no simple relationship to the rate constants of the dominant blocking reaction (cf., Aldrich et al., 1983).

Kinetics of MB^+ Binding

The kinetics of the MB^+ binding reaction cannot be ascertained until unequivocal evidence has been obtained as to the underlying mechanism of the blocking process. Two major questions must be answered to permit further resolution of MB^+ binding kinetics: Is drug binding state-dependent, and does the crayfish sodium pore show multi-ion properties that might influence drug binding? Our first step has been to look for evidence of product trapping as an indicator of state dependent block.

If drug block is significantly state dependent and if block of open channels is highly favored, one can predict a substantial shift in the equilibrium of channel activation (a shift to the left of the m_∞ vs. E_m distribution). At negative test potentials, product trapping by MB^+ will pull through many more channels than would have otherwise been activated in the absence of drug. Thus, the actual fraction of pores blocked may be several fold greater than the p value calculated from the control record. We have looked for this effect using tail current magnitude to assess the fractional MB^+ binding to the open state of the sodium channels. In Fig. 8 *B* the voltage dependence of MB^+ tail current magnitude is compared with two separate estimates of the voltage dependence of activation (Q_{ON}/Q_{ON} max and G_{Na}/G_{Na} max) obtained from this same pronased axon. At -40 mV the observed tail current is some threefold larger than would have been predicted, which provides substantial evidence of product trapping. We conclude that MB^+ binding must be partially, or fully, state dependent.

This conclusion renders inappropriate the pseudo–first-order analysis presented earlier (see Results), but does provide explanations for some of the anomalous findings of that approach. For example, the steep voltage dependence of the calculated k at negative membrane potentials (see Fig. 12 *A*) arises from the low p values and slow τ_{MB} measurements obtained in this voltage range. Both of these effects are predictable consequences of a state-dependent system, and will be particularly pronounced where the activation process has greatest voltage sensitivity. At negative potentials, the observed MB^+ kinetics will be seriously contaminated by the activation process. However, at more positive test potentials, the observed blocking kinetics will increasingly approach the limiting rate of the MB^+ binding reaction.

Our observations on MB^+ block at positive test potentials, where activation is nearly complete, suggest an asymmetric barrier placement and a drug binding site deep in the transmembrane voltage field (dz = 0.85). It is

encouraging that work by Horn et al. (1981) produced a similar estimate for the depth of the TMA^+ binding site ($dz = 0.89$), since their data from single channel recording should not be contaminated by axon kinetics. Unfortunately, due to the possible effects of ionic interactions within a multisite channel, any conclusion as to the depth of the drug binding site based on the effective valence of the blocking reaction may be premature (Hille and Schwarz, 1977). Although no direct evidence for multi-ion channel behavior has been reported from crayfish axons, evidence is acccumulating to suggest that squid axon sodium channels possess multiple ion binding sites (Begenisich and Cahalan, 1980*a*, *b*). Consistent with the occurrence of ionic interactions within a multisite pore, marked asymmetric effects of some blocking agents have been noted in both squid (Smith et al., 1983) and crayfish axons (Lo and Shrager, 1981*a*, *b*). By contrast, both in this study and in the pancuronium data of Yeh and Narahashi (1977), drug action was little affected by sodium current direction. Further work will thus be required to characterize the origins of the voltage sensitivity of MB^+ binding before any definitive conclusions can be drawn as to the position of this site within the transmembrane voltage field.

APPENDIX

In absence of any blocking drug, the simplified sequential reaction (Scheme II) would equilibrate with a fraction of channels in pre-open states (X_c), which may be defined as $p_1 = B/(B + A)$. Similarly, when the MB^+ blocking reaction is seen in isolation, the fraction of channels in the open and not blocked state(s) (X_o) is defined as $p_2 = l_o/(l_o + k_o)$. When the two reactions are then considered as a sequential system, the equilibrium for channel activation is shifted such that the fraction of channels left in the pre-open states (X_c) at equilibrium becomes $p'_1 = p_1/(p_1 + (1 - p_1)/p_2)$. It is clear that when $B \neq 0$, the addition of an open-channel, drug-blocking step will shift the equilibrium of channel activation towards the X_o and X_oMB states.

We wish to thank Dr. Brian Fellmeth for his computer programming assistance and to Linda Yoshida and Jane Inouye for their excellent secretarial assistance.

This work was performed with the support of the National Institutes of Health through research grant NSI7202 (to John G. Starkus) and GM29263 (to Martin D. Rayner). Additional support was also received from the University of Hawaii Research Council and in part by BRSG SO7 RR 07026 awarded by the Biomedical Research Support Grant Program, Division of Research Resources, National Institutes of Health.

Received for publication 21 September 1983 and in final form 9 April 1984.

REFERENCES

Aldrich, R. W., D. P. Corey, and C. F. Stevens. 1983. A reinterpretation of mammalian sodium channel gating based on single channel recording. *Nature* (*Lond.*). 306:436–441.

Armstrong, C. M., and R. S. Croop. 1982. Simulation of Na channel inactivation by thiazin dyes. *J. Gen. Physiol.* . 80:641–662.

Begenisich, T. B., and M. D. Cahalan. 1980*a*. Sodium channel permeation in squid axons. I. Reversal potential experiments. *J. Physiol.* (*Lond.*). 307:217–242.

Begenisich, T. B., and M. D. Cahalan. 1980*b*. Sodium channel permeation in squid axons. II. Non-independence and current-voltage relations. *J. Physiol.* (*Lond.*). 307:243–257.

Cahalan, M. D. 1978. Local anesthetic block of sodium channels in normal and pronase-treated squid giant axons. *Biophys. J.* 23:285–311.

Cahalan, M. D., and W. Almers. 1979*a*. Interactions between quaternary lidocaine, the sodium channel gates, and tetrodotoxin. *Biophys. J.* 27:39–56.

Cahalan, M. D., and W. Almers. 1979*b*. Block of sodium conductance and gating current in squid giant axons poisoned with quaternary strychnine. *Biophys. J.* 27:57–74.

Cahalan, M. D., B. I. Shapiro, and W. Almers. 1980. Relation between inactivation of sodium channels and block by quaternary derivatives of local anesthetics and other compounds. *Prog. Anesthesiol.* 2:17–33.

Coronado, R., and C. Miller. 1979. Voltage-dependent caesium blockade of a cation channel from fragmented sarcoplasmic reticulum. *Nature* (*Lond.*). 280:808–810.

Courtney, K. R. 1975. Mechanism of frequency-dependent inhibition of sodium currents in frog myelinated nerve by the lidocaine derivative GEA 968. *J. Pharmacol. Exp. Ther.* 195:225–236.

Dodge, F. A., and B. Frankenhaeuser. 1959. Sodium currents in the myelinated nerve fiber in *Xenopus laevis* investigated with voltage clamp technique. *J. Physiol.* (*Lond.*). 148:188–200.

French, R. J., and J. J. Shoukimas. 1981. Blockage of squid axon potassium conductance by internal tetra-*n*-alkylammonium ion of various sizes. *Biophys. J.* 34:271–291.

Glasstone, S., K. J. Laidler, and H. Eyring. 1941. The Theory of Rate Processes. McGraw-Hill, Inc., New York. 552–599.

Hille, B. 1977. Local anesthetics: Hydrophilic and hydrophobic pathways for the drug-receptor reaction. *J. Gen. Physiol.* 69:497–515.

Hille, B., and W. Schwarz. 1978. Potassium channels as multi-ion single-file pores. *J. Gen. Physiol.* 72:409–442.

Horn, R., J. Patlak, and C. F. Stevens. 1981. The effect of tetramethylammonium on single sodium channel currents. *Biophys. J.* 36:321–327.

Keynes, R. D., and E. Rojas. 1976. The temporal and steady-state relationships between activation of the sodium conductance and movement of the gating particles in squid giant axon. *J. Physiol.* (*Lond.*). 255:157–189.

Lo, M-V. C., and P. Shrager. 1981*a*. Block and inactivation of sodium channels in nerve by amino acid derivatives. I. Dependence on voltage and sodium concentration. *Biophys. J.* 35:31–43.

Lo, M-V. C., and P. Shrager. 1981*b*. Block and inactivation of sodium channels in nerve by amino acid derivatives. II. Dependence on temperature and drug concentration. *Biophys. J.* 35:45–57.

Oxford, G. S., and J. Z. Yeh. 1979. Interference with sodium inactivation gating in squid axons by internal monovalent cations. *Biophys. J.* 25(2, Pt. 2):195*a*. (Abstr.)

Rojas, E., and B. Rudy. 1976. Destruction of the sodium conductance inactivation by a specific protease in perfused nerve fibers from *Loigo*. *J. Physiol.* (*Lond.*). 262:501–531.

Schauf, C. L. 1983. Tetramethylammonium ions alter sodium channel gating in *Myxicola*. *Biophys. J.* 41:269–274.

Shrager, P. 1974. Ionic conductance changes in voltage clamped crayfish axons at low pH. *J. Gen. Physiol.* 64:666–690.

Smith, C., L. McKinney, M. Danko, and T. Begenisich. 1983. Monovalent and divalent guanidinium ions as probes of the sodium channel in squid giant axons. *Biophys. J.* 41(2, Pt. 2):144*a*. (Abstr.)

Starkus, J. G., and P. Shrager. 1978. Modification of slow sodium inactivation in nerve after internal perfusion with trypsin. *Am. J. Physiol.* 235(5):C238–244.

Starkus, J. G., B. D. Fellmeth, and M. D. Rayner. 1981. Gating currents in the intact crayfish giant axon. *Biophys. J.* 35:521–533.

Strichartz, G. R. 1973. The inhibition of sodium currents in myelinated nerve by quarternary derivatives of lidocaine. *J. Gen. Physiol.* 62:37–57.

Van Harreveld, A. 1936. A physiological solution for fresh water crustaceans. *Proc. Soc. Exp. Biol. Med.* 34:428–432.

Woodhull, A. M. 1973. Ionic blockage of sodium channels in nerve. *J. Gen. Physiol.* 61:687–708.

Yeh, J. Z. 1979. Dynamics of 9-aminoacridine block of sodium channels in squid axons. *J. Gen. Physiol.* 73:1–21.

Yeh, J. Z., and T. Narahashi. 1977. Kinetic analysis of pancuronium interaction with sodium channels in squid axon membranes. *J. Gen. Physiol.* 69:293–323.